# EVALUATION OF CFD TRANSITION MODELING FOR TRANSONIC, NATURAL-LAMINAR-FLOW DESIGN

James G. Coder<sup>1</sup>

<sup>1</sup>The Pennsylvania State University, University Park, PA 16801, United States

#### **Abstract**

A critical evaluation of prominent PDE-based laminar-turbulent transition models for CFD applications is presented. Several variants of the Amplification Factor Transport (AFT) modeling framework, along with a Local-Correlation Transition Model, are assessed. As the baseline models are anchored to incompressible considerations, candidate compressibility corrections are presented for the AFT models. A crossflow transition extension is included with all the models; however, this is de-emphasized in favor of streamwise mechanisms in the present study. The models are applied to test cases of varying complexity to test their accuracy for capturing the movement of transition with changing angle of attack and their sensitivity to varying Mach numbers in the near-sonic regime, both of which are crucial details for using such transition models for natural-laminar-flow design in the transonic regime. It is ultimately found that the AFT2014 model with a compressibility correction performs best, providing accurate solutions and exhibiting the desired behavior in the presence of changing lift and changing Mach number.

Keywords: transition, natural laminar flow, aerodynamics, CFD, aircraft design

## 1. Introduction

Natural-laminar-flow (NLF) wing design for aircraft operating in the transonic flight regime presents a tremendous opportunity for reducing fuel/energy consumption, thereby reducing operational costs and lessening the environmental impact of aviation. NLF design in this regime has been studied for a wide range of aircraft, achieving different levels of maturity. For example, the HondaJet HA-420 is a light business jet with an NLF wing [1] that is in production. Numerous NLF design studies have been performed for regional jet and smaller narrow-body aircraft, such as the Boeing "SUGAR High" transonic truss-braced wing (TTBW) [2, 3], the DLR LamAIR and TuLAM/EcoWing forward-sweptwing concepts [4, 5], and the MIT/Aurora D8.5 "Double Bubble" [6]. More aggressive design studies have targeted large, wide-body aircraft, such as the NASA Common Research Model with Natural Laminar Flow (CRM-NLF) [7, 8] and the accompanying crossflow-attenuated NLF (CATNLF) design methodology [9].

Necessary to support such design studies is accurate and robust aerodynamic design and analysis tools that account for the relevant laminar-turbulent transition mechanisms (i.e., Tollmien-Schlichting / streamwise instabilities, crossflow instability, attachment line instability, etc.) to predict the extent of laminar flow. Based on Ref. [1], a predominately 2D wing design method was used with an inverse design and panel-method/integral-boundary-layer tool. TuLAM and related projects use a '2.75D' inverse design methodology to achieve target pressure distributions that provide desired boundary-layer stability characteristics. While RANS flow solvers are included in the design loop, boundary-layer transition predictions are handled using a specialized external tool [10]. The CATNLF

methodology used to design CRM-NLF wing is conceptually similar, where a RANS solver is coupled to external boundary-layer tools [9]. Target pressure distributions are specified by the designer, and the CDISC methodology is used to update the geometry [9].

The common trait of the tools used in the aforementioned design studies is the presence of an external, non-RANS boundary-layer solver to predict the transition locations. This is unsurpising, as such tools embody the current state of the art in transition prediction. Nevertheless, such methods can create significant bottlenecks in the design process and in generating aircraft performance databases. Trustworthy boundary-layer stability codes for swept, tapered wings are not widely available across the industry, creating a barrier of entry for new efforts. Some options exist from government agencies, such as NASA in the United States, but these often come with citizenship restrictions. Even then, substantial labor investment is required to either have a person in the loop for every analysis point, or to develop and debug an automation process.

An appealing alternative is to make use of PDE-based transition models that are available in many commercial and government RANS computational fluid dynamics (CFD) codes. Such models offer the possibility of "care free" application that fits within an industrial CFD workflow; however, they are approximations and abstractions of the aforementioned stability tools, and are thus qualify as reduced-order models. Yet, this should not be taken as undermining the utility of PDE-based models for aerodynamic design. With appropriate understanding of the models' strengths and weaknesses, trust can be built for their application to emerging aircraft design concepts and building necessary performance databases.

The objective of this paper is to provide a critical evaluation of several prominent PDE-based transition models for use in aerodynamic design. The models being considered are the Coder Amplification Factor Transport (AFT) modeling framework [11, 12, 13] and the Langtry-Menter local-correlation transition model (LCTM) [14, 15], as they and related models are available in numerous government and commercial CFD codes. These models were developed primarily based on incompressible arguments, which is known to have an adverse effect on prediction accuracy [16]. Therefore, two compressibility corrections for the AFT model are presented and considered in this work. Four test cases are considered, all of which have available experimental data for validation. These include 1) a low-speed NLF airfoil to understand the predictive accuracy in the absence of appreciable compressibility effects; 2) a body of revolution at high-Mach, near-sonic conditions to evaluate the effect of Mach number in the absence of shockwave interactions; 3) a transonic slotted, NLF wing for which extensive IR thermographic measurements of boundary-layer transition are available for varying Mach number, Reynolds number, and angle of attack; and 4) the CRM-NLF wing at on-design conditions.

## 2. Transition Models

## 2.1 AFT2019b

The first PDE-based boundary-layer transition model is the 2019b variant of the Amplification Factor Transport (AFT) modeling framework [12, 13]. The basis of the AFT model is the construction of local estimates of integral boundary-layer parameters. The estimated integral parameters are then used to evolve a model for the growth rate of the instability envelope amplification factor  $\tilde{n}$ . While such models are typically defined along the surface streamline, the AFT model expresses this process as a field PDE,

$$\frac{\partial \rho \tilde{n}}{\partial t} + \frac{\partial \rho u_j \tilde{n}}{\partial x_j} = \rho \Omega F_{crit} F_{growth} \frac{d\tilde{n}}{dRe_{\theta}} + \frac{\partial}{\partial x_j} \left[ \sigma_n \left( \mu + \mu_t \right) \frac{\partial \tilde{n}}{\partial x_j} \right]$$
(1)

In this expression, the  $F_{crit}$  function reflects the cut-in of instability growth at the critical value of  $Re_{\theta}$ ,  $F_{growth}$  reflects the streamwise growth of the boundary-layer, and  $\frac{d\tilde{n}}{dRe_{\theta}}$  provides the non-dimensionalized growth rate of the instability envelope. All of these functions depend on the integral  $H_{12}$  shape factor, which is estimated using

$$H_{12} = f(H_L), \quad H_L = \frac{\rho d_{wall}^2}{\mu} \frac{\partial}{\partial x_i} \left( u_j \frac{\partial d_{wall}}{\partial x_j} \right) \frac{\partial d_{wall}}{\partial x_i}$$
 (2)

This form of  $H_L$  is based on the local shape factor proposed by Menter and Smirnov [17], and uses the wall-normal gradient of the wall-normal velocity as a surrogate for  $\frac{\partial u}{\partial x}$ . This is perfectly valid for incompressible flows by virtue of continuity, but it becomes less true as Mach number increases. An earlier version of the model, termed AFT2017 [18], used the momentum gradient, but was ultimately replaced with velocity gradient. No correction factors for compressibility are included in the AFT2019b model.

In tandem with the amplification factor transport equation is a transport equation for a modified intermittency variable,  $ga\tilde{m}ma = \ln \gamma$ , where the unmodified  $\gamma$  is a binary logic variable describing whether the local flow is laminar ( $\gamma \to 0$ ) or turbulent ( $\gamma = 1$ ). The resulting transport equation takes the form,

$$\frac{\partial \rho \tilde{\gamma}}{\partial t} + \frac{\partial \rho u_j \tilde{\gamma}}{\partial x_j} = c_1 \rho S F_{onset} \left[ 1 - \exp \tilde{\gamma} \right] - c_2 \rho \Omega F_{turb} \left[ c_3 \exp \tilde{\gamma} - 1 \right] + \frac{\partial}{\partial x_j} \left[ (\mu + \sigma_y \mu_t) \frac{\partial \tilde{\gamma}}{\partial x_j} \right]$$
(3)

The AFT2019b model works in tandem with the one-equation eddy-viscosity model of Spalart and Allmaras [19]. Details of the function definitions, calibration constants, and coupling with the eddy-viscosity model can be found in Ref. [13].

# 2.2 Langtry-Menter 2009

The second major laminar-turbulent model considered the Local Correlation Transition Model (LCTM) of Langtry and Menter [14]. At it's core, the Langtry-Menter model is based on using Holstein-Bohlen pressure gradient parameter,

$$\lambda_{\theta} = \frac{\rho \, \theta^2}{\mu} \frac{dU_e}{ds} \tag{4}$$

and the turbulence intensity to estimate a local transitional value of the momentum-thickness Reynolds number,  $Re_{\theta t} = f(\lambda_{\theta}, Tu)$ . It implements this concept by transporting a  $\widetilde{Re_{\theta t}}$  variable through the domain,

$$\frac{\partial \rho \widetilde{Re_{\theta t}}}{\partial t} + \frac{\partial \rho u_j \widetilde{Re_{\theta t}}}{\partial x_j} = P_{\theta t} + \frac{\partial}{\partial x_j} \left[ \sigma_{\theta} \left( \mu + \mu_t \right) \frac{\partial \widetilde{Re_{\theta t}}}{\partial x_j} \right]$$
 (5)

Outside the boundary layer, the governing PDE attracts  $\widetilde{Re}_{\theta t}$  to a local estimate of  $Re_{\theta t}$  as calibrated at the edge of the boundary layer. Inside the boundary layer, the attractor is suppressed, and the edge value diffuses toward the wall.

 $\widetilde{Re_{ heta t}}$  is supplemented by an intermittency transport equation of the form,

$$\frac{\partial \rho \gamma}{\partial t} + \frac{\partial \rho u_j \gamma}{\partial x_j} = P_{\gamma} - E_{\gamma} + \frac{\partial}{\partial x_j} \left[ \left( \mu + \frac{\mu_t}{\sigma_f} \right) \frac{\partial \gamma}{\partial x_j} \right]$$
 (6)

As with the AFT2019b model, the transported intermittency is a binary logic variable and is not intended to represent the physical intermittency in the flow.

The Langtry-Menter LCTM is coupled with the Menter Shear-Stress Transport (SST)  $k-\omega$ , two-equation, eddy-viscosity model [20]. No explicit corrections are included in the model for compressibility effects.

#### 2.3 AFT2014

Also under consideration in this work is the original version of the AFT model by Coder and Maughmer [11], now termed AFT2014. The AFT2014 model is based on a different local shape factor than AFT2019b,

$$H_L = \frac{d_{wall}\Omega}{U_e} \tag{7}$$

where  $d_{wall}$  is the distance to the nearest wall,  $\Omega$  is the vorticity magnitude, and  $U_e$  is the velocity at the edge of the boundary layer. While in the strictest sense  $U_e$  is a non-local quantity, it can be well-estimated based on the local pressure and the free-stream total enthalpy (which is a static parameter

of a steady simulation and thus does not require search operations) using,

$$\frac{U_e^2}{2} + \frac{\gamma}{\gamma - 1} \frac{P}{\rho_e} = \frac{U_\infty^2}{2} + \frac{\gamma}{\gamma - 1} \frac{P_\infty}{\rho_\infty} \tag{8}$$

$$\rho_e = \rho_\infty \left(\frac{P}{P_\infty}\right)^{1/\gamma} \tag{9}$$

The closure for  $\rho_e$  assumes isentropic flow outside of the boundary layer. For transonic, fixed-wing applications, this is considered to be a reasonable assumption so long as the region of interest for laminar-turbulent transition is upstream of any shockwaves. Even so, the shockwaves in on-design transonic cases is generally weak and itself a cause of transition, thus mitigating errors.

For the specific implementation used in this work, the  $\gamma$  transport equation from the AFT2019b model is used in conjunction with the AFT2014  $\tilde{n}$  equation and accompanying correlations and calibration constants.

# 2.4 AFT2014Comp

As will be seen in the subsequent sections, the standard versions of the AFT models do not respond appropriately to varying Mach number at the boundary-layer edge. There are multiple contributing factors to this behavior, including:

- Error in estimation of integral shape factor  $(H_{12} \text{ and/or } H_k)$  based on local quantities
- Static dependency of  $Re_{ heta,0}$  and  $rac{d ilde{n}}{dRe_{ heta}}$  on shape factor across all Mach numbers

The first deficiency is a result of the correlations used to construct the AFT model, the baseline form of which is based on Falkner-Skan solutions. For the AFT2014 model, the maximum value attained by the  $H_L$  local shape factor in the boundary layer increases with Mach number. Thus, the **Version 1** (v1) compressibility correction is to modify

$$H_k = \frac{H_{12,original}}{1 + 0.031M_e^2} \tag{10}$$

and retain the original transition correlations. By doing so, the estimated shape factor (more akin to the kinematic shape factor  $H_k$  than the standard  $H_{12}$  shape factor) retains a value closer to its incompressible value (and actually slightly lower). While this does not match the actual kinematic shape factor (in fact, the original AFT2014 correlation for  $H_{12}$  tracks very well with  $H_k$  across a wide range of Mach numbers), it allows the transition correlations to at least retain their incompressible behaviors.

The second deficiency arises from the underlying approximate envelope method. The baseline AFT models employ the correlations as implemented in recent versions of XFOIL and MSES [21], and are rooted in incompressible behavior. A notable compressibility modification is the one proposed by Sturdza [22] for supersonic natural-laminar-flow design. Drawing from Sturdza's correlations for adiabatic walls [22] and observations made by Venkatachari et al. [16], the **Version 2** (v2) compressibility correction is to retain the AFT2014 estimate of the integral shape factor (taken to be the kinematic shape factor) and modify  $Re_{\theta,0}$  and  $\frac{d\tilde{n}}{dRe_0}$  as,

$$\log_{10}\left(\frac{Re_{\theta,0}}{K_0}\right) = 0.7 \tanh\left(\frac{14}{H_k - 1} - 9.24\right) + \frac{2.492}{(H_k - 1)^{0.43}} + 0.62 \tag{11}$$

$$\frac{d\tilde{n}}{dRe_{\theta}} = \frac{0.01}{K_b} \left[ 2.8 \left( H_k - 1 \right) - 3.45 \exp \left[ -\left( \frac{3.87}{H_k - 1} - 2.52 \right)^2 \right] + 2.4 K_a + 2.5 K_w \tanh \left( 1.5 \left( H_k - 3.1 \right) \right) + K_c \right]$$
(12)

with

$$K_0 = \frac{2}{\pi} \arctan(10K_w) + 1$$
 (13)

$$K_a = 0.2H_k (H_k - 2.5911) \frac{K_w}{K_w + 1}$$
(14)

$$K_b = 4.7K_w + 1 ag{15}$$

$$K_c = 1.2K_w^{3/2} \tag{16}$$

and

$$K_w = \sqrt{Pr} \frac{\gamma - 1}{2} M_e^2 \tag{17}$$

The construction of  $K_w$  is based on the adiabatic wall temperature with a recovery factor based on Prandtl number. The value of edge Mach number  $M_e$  is based on quantities already used in the AFT2014 model,

$$M_e^2 = \frac{\rho_e U_e^2}{\gamma P} \tag{18}$$

A comparison of the baseline model with the v1 and v2 compressibility corrections, all based on nominal values of  $H_k$ , are plotted in Fig. 1 along with the Sturdza correlations [22]. The goal for the v1 correction has been achieved, where now increasing the Mach number suppresses both the onset and the growth rate of instabilities; however, the physicality of this is not validated. The v2 correction is based more rigorously on stability results (see Ref. [22]), and shows more aggressive damping of the growth rate, but a trend reversal around  $M_e = 0.8$  on the behavior of  $Re_{\theta,0}$ . This behavior is inherited from the underlying Sturdza model; however, the current implementation follows Venkatachari et al. [16] and neglects the influence of a running  $H_k$  average.

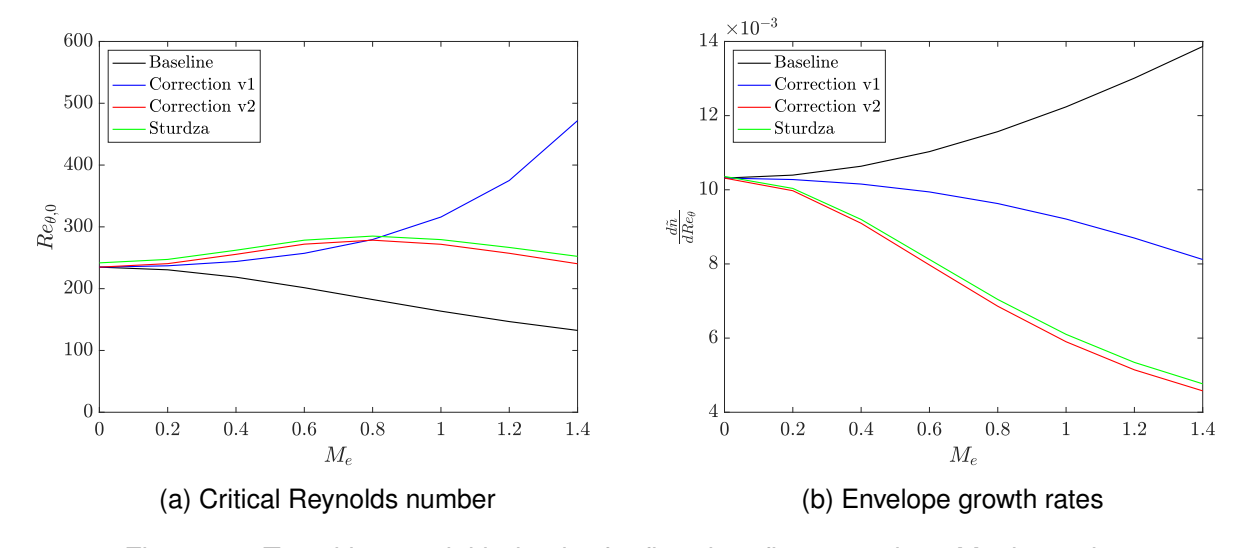


Figure 1 – Transition model behavior for flat-plate flow at various Mach numbers.

## 2.5 Crossflow Extension

All models considered here include a crossflow transition extension based on the model of Langtry et al. [15]. This formulation is based on the local helicity in the boundary layer along with correlations based on a prescribed surface roughness. The implementation with the AFT-based models follows that laid out by Carnes and Coder [13].

## 2.6 Turbulence Indices

A useful tool for identifying where laminar-turbulent transition happens in a CFD simulation is to use the so-called "turbulence index". Whereas other flow quantities, such as surface skin friction or transported intermittency, can be potentially misleading about the transition location, turbulence indices exploit the analytical near-wall behavior of the transition-sensitized turbulence models to determine if the local boundary layer is turbulent.

As the AFT models used in this work are coupled to the Spalart-Allmaras turbulence model, it is appropriate to use Spalart's turbulence index [19],

$$i_{t,SA} = \frac{1}{\kappa u_{\tau}} \frac{\partial \tilde{v}}{\partial n} \tag{19}$$

For the Langtry-Menter solutions, the index developed by Carnes and Coder [23] is used,

$$i_{t,LM} = \frac{6.1}{u_{\tau}^{2.346}} \frac{d\left(vk^{0.673}\right)}{dy} \tag{20}$$

The reader should be aware that the Langtry-Menter model sufficiently alters the near-wall behavior of the SST model such that the standard SST turbulence index is no longer useful.

#### 3. Flow Solver

The flow solver used in this study is the OVERFLOW 2.4b code developed by NASA Langley [24]. While the release version of the code features the AFT2019b and Langtry-Menter transition models, custom modifications were made by the author to extend the AFT2019b model to include crossflow transition (AFT2019b+CF) and to implement the AFT2014+CF and AFT2014comp+CF models.

All simulations included in this paper employ MUSCL-type reconstructions for the inviscid fluxes for all equations. The mean-flow uses a 3<sup>rd</sup>-order<sup>1</sup> method with the Koren limiter that reconstructs the 'left' and 'right' primitive variable states at the node midpoint locations. The Roe flux-difference-splitting scheme [25] is then used to construct finite-volume fluxes. The invisicid fluxes of the turbulence and transition models use velocity-based upwinding. All viscous fluxes are constructed using a 2<sup>nd</sup>-order-accurate formulation with a compact stencil. Non-time-accurate implicit time stepping with the LU-SGS algorithm of Yoon and Jameson [26] was used to converge the solutions.

## 4. Test Cases and Results

## 4.1 NLF(1)-0416, Natural-Laminar-Flow Airfoil

The first test case considered in this study is the NLF(1)-0416, natural-laminar-flow airfoil, designed by Somers based on requirements derived from general aviation aircraft and subsequently tested in the NASA Langley Low-Turbulent Pressure Tunnel (LTPT) [27]. This airfoil has been previously identified as a useful test case for CFD transition modeling, as its intended Reynolds number range is representative of many inhabited flight vehicles, and the primary transition mechanism is expected to be natural transition via Tollmien-Schlichting instabilities as opposed to laminar separation bubbles [28]. The specific test conditions are described in Table 1. Although this case is low-Mach number and far from the transonic regime, it provides an important baseline for the predictive capabilities of the transition models. The fine-resolution structured, overset grid from the First AIAA CFD Transition Modeling and Prediction Workshop  $^2$  is used here. This grid features a C-topology with 769 points on the surface and 145 points in the wake cut, along with 145 wall-normal points that have an initial spacing of  $2.1 \times 10^{-6}c$  (target  $\Delta y^+ \approx 1/3$ ).

The drag polars predicted using the three low-speed transition models are plotted in Fig. 2 along with experimental measurements obtained from LTPT [27]. The AFT models capture both the qualitative

<sup>&</sup>lt;sup>1</sup>The stated accuracy is based on 1-dimensional analysis. In 2 and 3 dimensions, it reduces to 2<sup>nd</sup>-order accuracy.

<sup>&</sup>lt;sup>2</sup>https://transitionmodeling.larc.nasa.gov/workshop i/

Table 1 - NLF(1)-0416 Run Conditions

Parameter	Value(s)
Mach Number	0.1
Angle of Attack	$[-4^{\circ}, 8^{\circ}]$ in $2^{\circ}$ increments
Chord Reynolds Number	$4 \times 10^6$
Freestream Turbulence Intensity	0.15%
Critical Amplification Factor	7.2

character of the drag curve quite well, and with strong quantitative agreement as well. Near minimum drag ( $c_l \approx 0.5$ ), the AFT2019b model predicts the drag value more accurately than AFT2014b; however, AFT2014 does better at capturing the overall low-drag lift-coefficient range ( $0 \lesssim c_l \lesssim 1$ ), although it underpredicts drag at higher  $c_l$  values. Conversely, the Langtry-Menter model underpredicts the drag values and greatly overpredicts the extent of the low-drag lift-coefficient range.

From the perspective of aerodynamic design, the errors of the Langtry-Menter model are rather serious. Overprediction of the low-drag range can greatly mislead a designer or an optimizer, suggesting performance gains that are not achievable in reality. This is further reinforced by plotting the same data in terms of the lift-to-drag ratio as in Fig. 3. The Langtry-Menter model overpredicts the maximum  $c_l/c_d$  by 17.5%, whereas AFT2014 underpredicts it by only 0.02% and AFT2019b underpredicts it by 5.5%. A contributing factor to the Langtry-Menter model's behavior is the phenomenon of free-stream turbulence decay, which is an inherent (and intended) property of the underlying SST turbulence model unless so-called sustaining terms are used [29, 30]. For internal flows, such as for turbomachinery, the free-stream turbulence decay is well-justified, but for external flows with effectively infinite domains, it results in contradictions such as predicting effectively zero FSTI over the body and/or requiring infinite eddy-viscosity ratios. While the former scenario is not problematic in the fully turbulent mode as the SST model was designed to be resilient to free-stream conditions, it causes the model correlations to bottom out at the lowest permissible turbulence intensity and thus removes it as a useful independent parameter. The latter scenario contaminates the laminar boundary layer and leads to incorrect predictions.

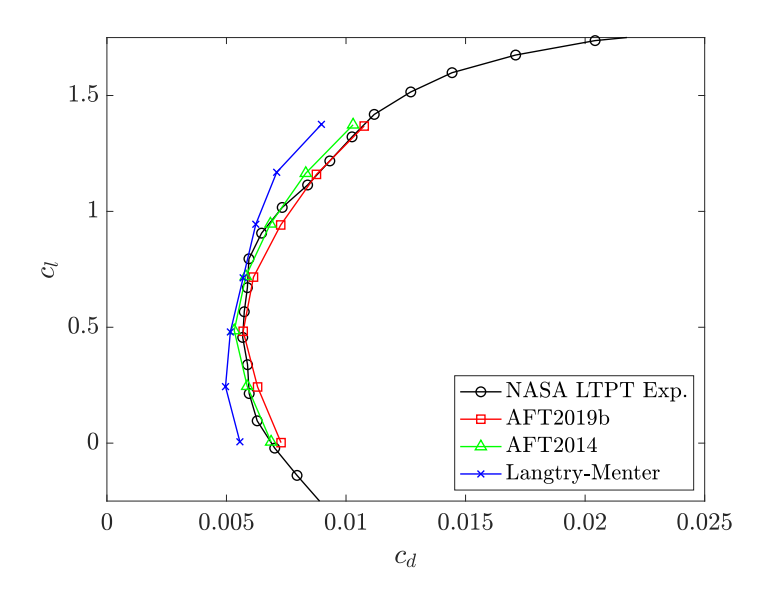


Figure 2 – Comparison of experimental [27] and predicted drag polars for NLF(1)-0416 airfoil,  $Re = 4 \times 10^6$ .

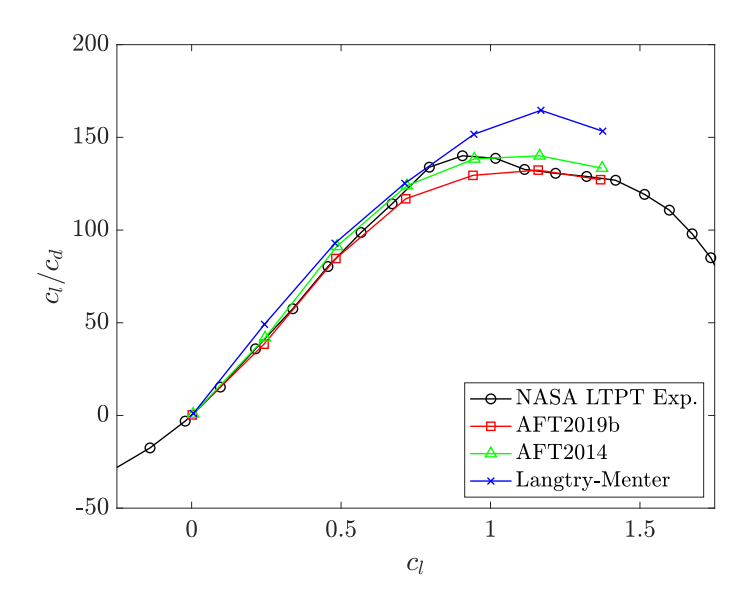


Figure 3 – Comparison of experimental [27] and predicted lift-to-drag ratios for NLF(1)-0416 airfoil,  $Re = 4 \times 10^6$ .

# 4.2 NASA Ames Body of Revolution

The second test case considered in this study is a body of revolution with fineness ratio 7.5 originally tested by Boltz et al. in the NASA Ames 12-ft pressure tunnel [31]. Geometric details of the model are provided in Ref. [31] along with transition locations (inferred from surface temperature measurements) at a Reynolds number of  $9 \times 10^6$  (based on a reference length of 8 ft) for M=0.60, 0.71, 0.81, and 0.91. Free-stream turbulence intensity in the tunnel is reported to be less than 0.02%. Mack's relation for critical amplification factor suggests  $N_{crit}\approx 12$ ; however, linear stability analyses have suggested a lower value of  $N_{crit}\approx 6.3.^3$ . Thus, this value is used as the baseline for AFT-based simulations, whereas the Langtry-Menter model was run with  $Tu_\infty=0.21603\%$  for the sake of consistency with the AFT solutions. As the test was performed with no incidence and no sideslip on the model, the simulations performed here are axisymmetric.

The predictions from the AFT2019b, AFT2014, Langtry-Menter, and the AFT2014 model with the compressibility corrections are plotted in Fig. 4 with experiment. Some very notable trends emerge from these data. Most notably, the AFT2019b and Langtry-Menter models exhibit no appreciable sensitivity to Mach number for this case, and the resulting transition locations do not vary. Of these two, the AFT2019b model predicts a transition location more consistent with the experimental reference, whereas the Langtry-Menter model predicts transition far downstream. As with the previous test case, this behavior of the Langtry-Menter model is attributed to the free-stream turbulence decay causing the transition correlation to "bottom out" at its lower-Tu limit. The AFT2014 model (without any compressibility corrections) captures some sensitivity to Mach number with the correct sign to the curve's slope, although the sensitivity is greatly reduced compared to experiment. Moreover, the AFT2014 model predicts transition far upstream, but this is consistent with the idea that compressibility tends to stabilize the boundary layer in the Mach number regime of interest. The two compressibility corrections applied to the AFT2014 model greatly improve the quality of the predictions and capture the Mach-number sensitivity much more consistently with experiment. The v1 correction shows the strongest agreement with experiment, slightly underpredicting the amount of laminar flow, whereas the v2 correction overpredicts the amount of laminar flow. For both of these, quantitative agreement can be improved by adjusting the specified  $N_{crit}$ ; however, one should exercise caution in doing so.

<sup>&</sup>lt;sup>3</sup>Private communications

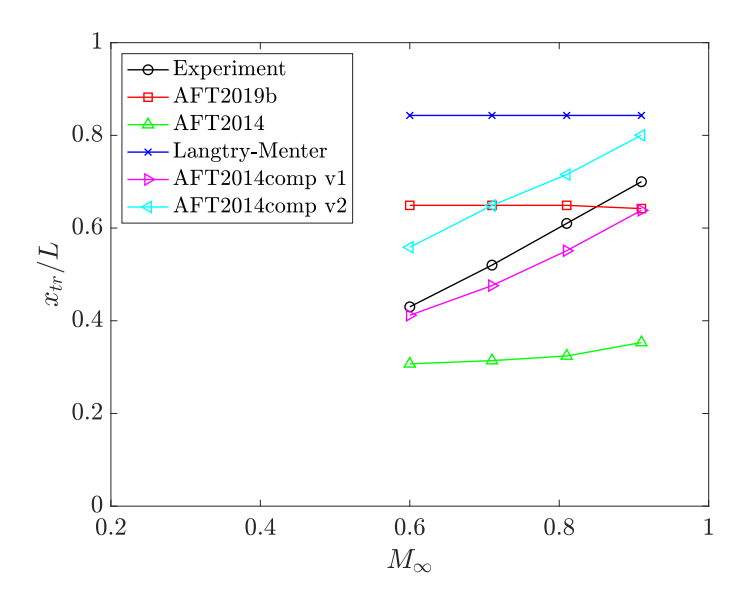


Figure 4 – Comparison of measured and predicted transition locations for fineness-ratio 7.5 body of revolution at various Mach numbers.

# 4.3 Slotted, Natural Laminar Flow Wing

A recent effort funded by the NASA University Leadership Initiative explored the benefits of slotted, natural-laminar-flow (SNLF) airfoils and wings as an enabling technology to meet far-term goals for reducing energy consumption of commercial aircraft. A product of this effort is the S207, SNLF airfoil designed by Somers [32, 33] using requirements derived from a reference 150-passenger transonic, truss-braced wing configuration. The S207 served as the basis for a swept, semi-span wing that was tested in the NASA Ames 11-ft Transonic Wind Tunnel [34] 4. The wind-tunnel model is untwisted with a constant airfoil section (S207), constant sweep of 12.5°, and constant chord of 24 inches with a 6-ft span. A key product of the test is boundary-layer transition data obtained using four infrared cameras, two on each the upper and lower surfaces of the main element. This was facilitated by the model being painted with a low-emissivity black paint that was finished to a roughness of  $R_a < 20 \times 10^{-6}$  inches as measured using a profilometer during test preparation. Testing was performed at a wide range of Mach and Reynolds numbers that cover the conditions anticipated for the TTBW reference aircraft while also documenting the limits for which laminar flow can be achieved for this geometry. Primary focus of the current study is the ability to predict the upper limit of the low-drag lift-coefficient range with varying Mach and Reynolds number. Specific conditions are described in Table 2. For all CFD simulations, a critical amplification factor of 9 (equivalent to Tu = 0.07%) was used, and the crossflow roughness parameter was set to the pre-test measured value; however, transition for this case are expected to be dominated by streamwise instability mechanisms.

Table 2 – SNLF Wing Run Conditions

Case	Mach Number	<b>Chord Reynolds Number</b>	Angle of Attack
Run 221	0.700	$12 \times 10^{6}$	0°, 1°
Run 240	0.700	$10 \times 10^{6}$	$0^{\circ}$ , $1^{\circ}$
Run 242	0.750	$10 \times 10^{6}$	1°, 2°
Run 243	0.775	$10 \times 10^{6}$	$1^{\circ}$ , $2^{\circ}$

Predicted upper-surface transition behaviors for "Run 221" using the AFT2019b+CF, AFT2014+CF, and AFT2014Comp-v1+CF are plotted in Figs. 5 and 6 for 0° and 1° angles of attack, respectively. Also include are IR thermographic images taken during the wind-tunnel test, and show roughly the

<sup>&</sup>lt;sup>4</sup>S207 geometry available under license by Airfoils, Incorporated. Wind-tunnel data available from author upon reasonable request

mid-span of the model. In the IR images, transition is evident by sharp gradients resulting from differential heat-transfer rates. For  $\alpha=0^\circ$ , there are several turbulent wedges present in the flow, but no ascertainable transition front upstream of the trailing edge of the fore element. The AFT models without sensitization to compressibility effects predict transition to be upstream of mid-chord, whereas the AFT2014Comp-v1+CF model predicts it to be much further aft, particularly inboard. At  $\alpha=1^\circ$ , the IR image shows a definitive transition front at approximately mid-chord of the fore element (approximately 40% of the overall chord). The AFT2019b and AFT2014 models predict transition to be much closer to the leading edge, whereas the AFT2014Comp-v1+CF model places it closer to mid-chord in line with the experiment.

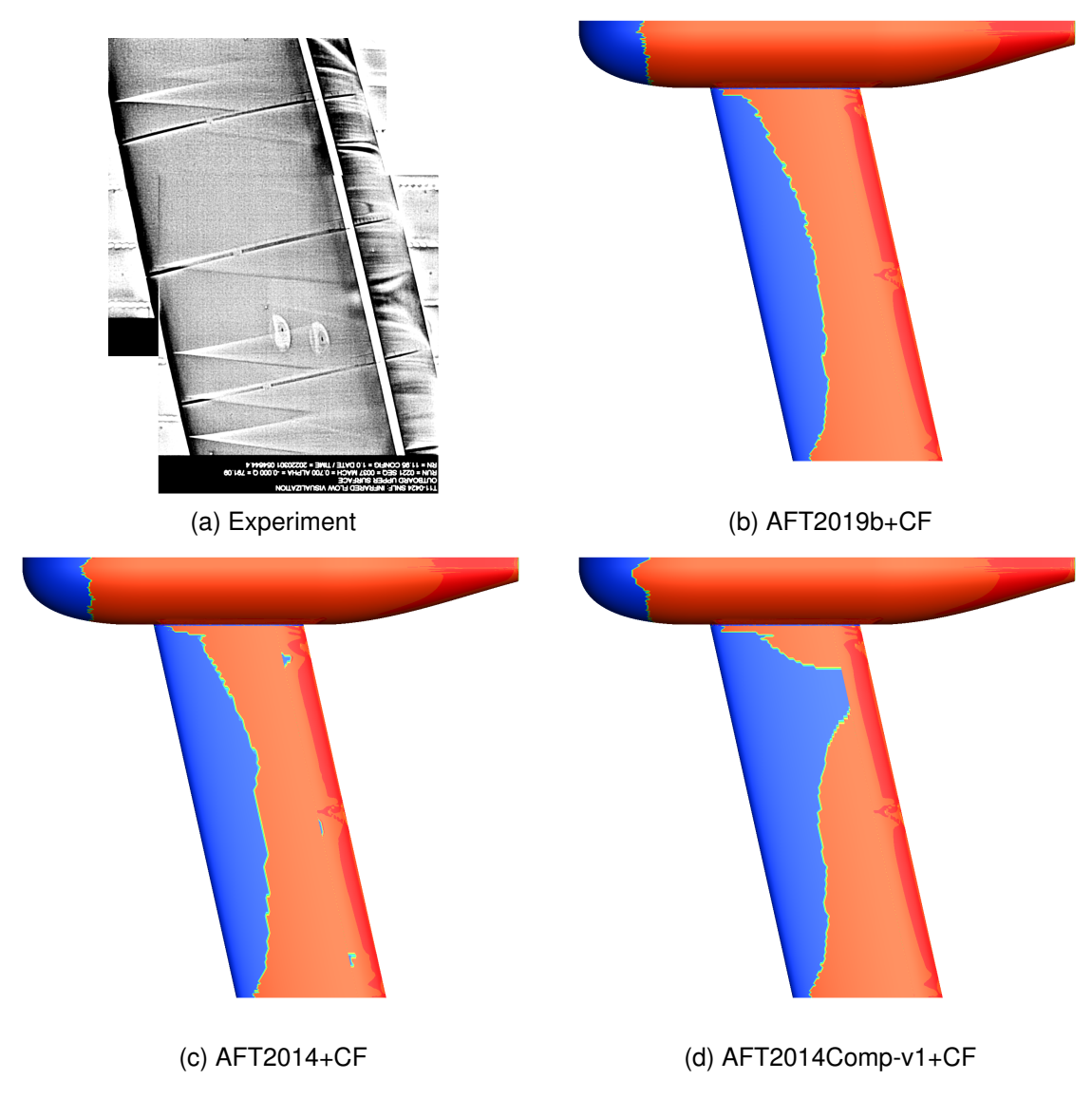


Figure 5 – Transition behavior of the SNLF wing predicted by the AFT model variants for M=0.70,  $Re=12\times10^6$ , and  $\alpha=0^\circ$ .

A similar comparison for "Run 243" is included as Figs. 7 and 8, except the AFT2019b+CF results have been replaced with the Langtry-Menter model. This case is at an appreciably higher Mach number of M=0.775, which places the test conditions firmly in the transonic regime. For  $\alpha=1^\circ$ , the IR image shows laminar flow over the full extent of the fore element for most of the field of view, with a transition front visible towards the bottom of the subfigure (corresponding to the outbard edge of the field of view). Both the Langtry-Menter and the AFT2014Comp-v1 models predict extensive laminar flow in this region, whereas the AFT2014 model predicts a premature transition front. For  $\alpha=2^\circ$ , the experimental measurements show the presence of inboard and outboard transition fronts, with full-extent laminar flow in the center of the field of view. Langtry-Menter and the AFT2014Comp-v1

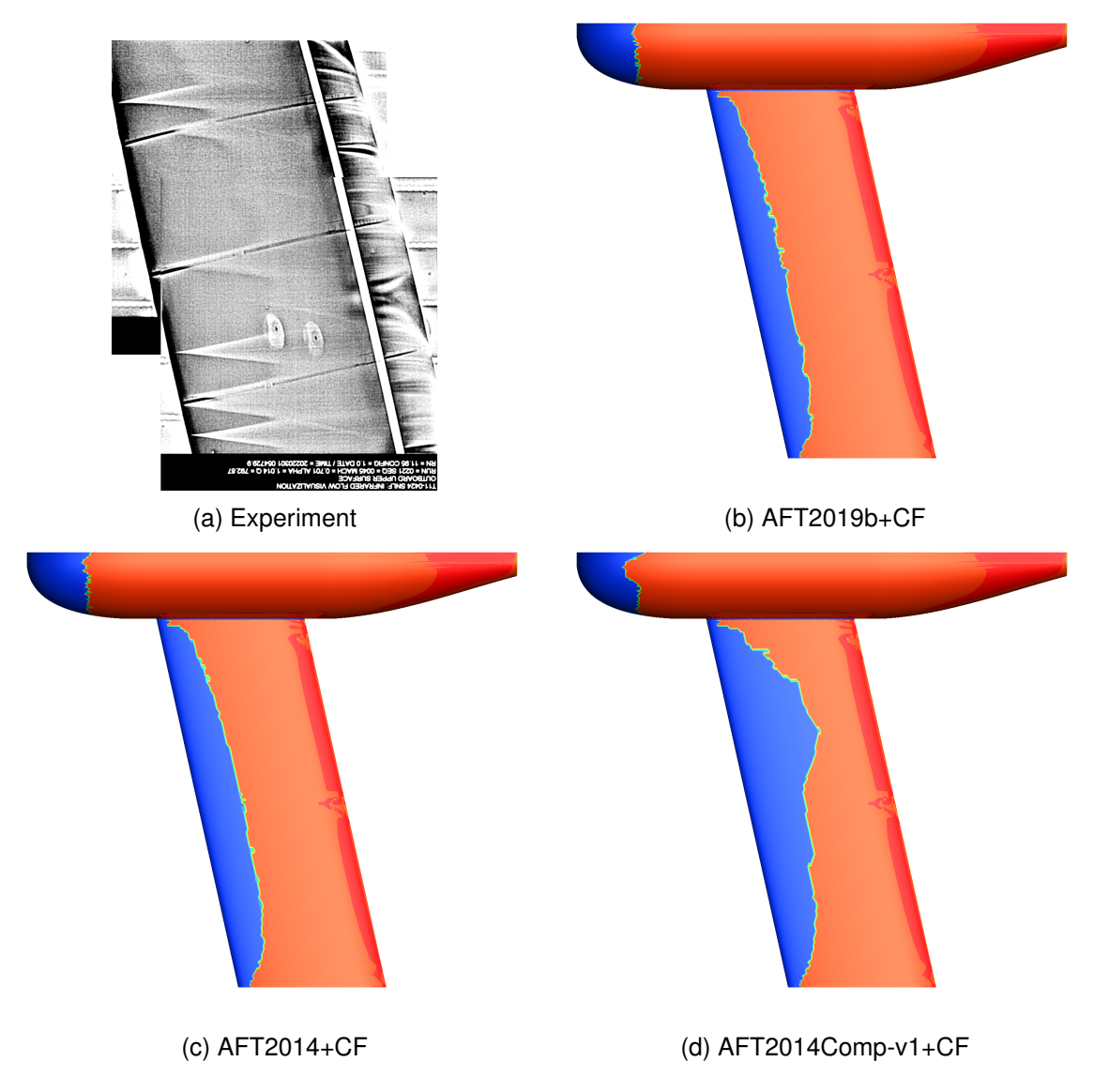


Figure 6 – Transition behavior of the SNLF wing predicted by the AFT model variants for M=0.70,  $Re=12\times10^6$ , and  $\alpha=1^\circ$ .

capture this behavior reasonably well, as transition in the simulations is induced by shockwaves. For the AFT2014 model, transition occurs upstream of the shockwave except for near the wing tip.

# 4.4 NASA Common Research Model with Natural Laminar Flow (CRM-NLF)

The final test case considered here is the natural-laminar-flow variant of the NASA Common Research Model, termed the CRM-NLF [7]. This configuration was designed using a strategy known as crossflow-attenuated NLF (CAT-NLF) with the intent of demonstrating extensive laminar flow for conditions representative of a large commercial transport [9]. The design was experimentally tested in the NASA National Transonic Facility (NTF) at cryogenic conditions to achieve full-scale Mach and Reynolds numbers [8]. Transition measurements were obtained optically through the use of temperature sensitive paint. The CRM-NLF geometry and test data were also included as a test case in the First AIAA CFD Transition Modeling and Prediction Workshop. While the workshop prescribed analyses at 4 angles of attack for M=0.86 and  $Re=15\times10^6$ , the present study focuses only on the "on-design"  $\alpha=2^\circ$  case due to computational resource limitations. The committee-provided Rev0 L3 structured, overset grid was used for the computations.

The predicted transition behaviors for the AFT2019b+CF, AFT2014Comp+CF, and Langtry-Menter models are shown in Fig. 10. The overall behaviors of the predicted transition fronts are similar

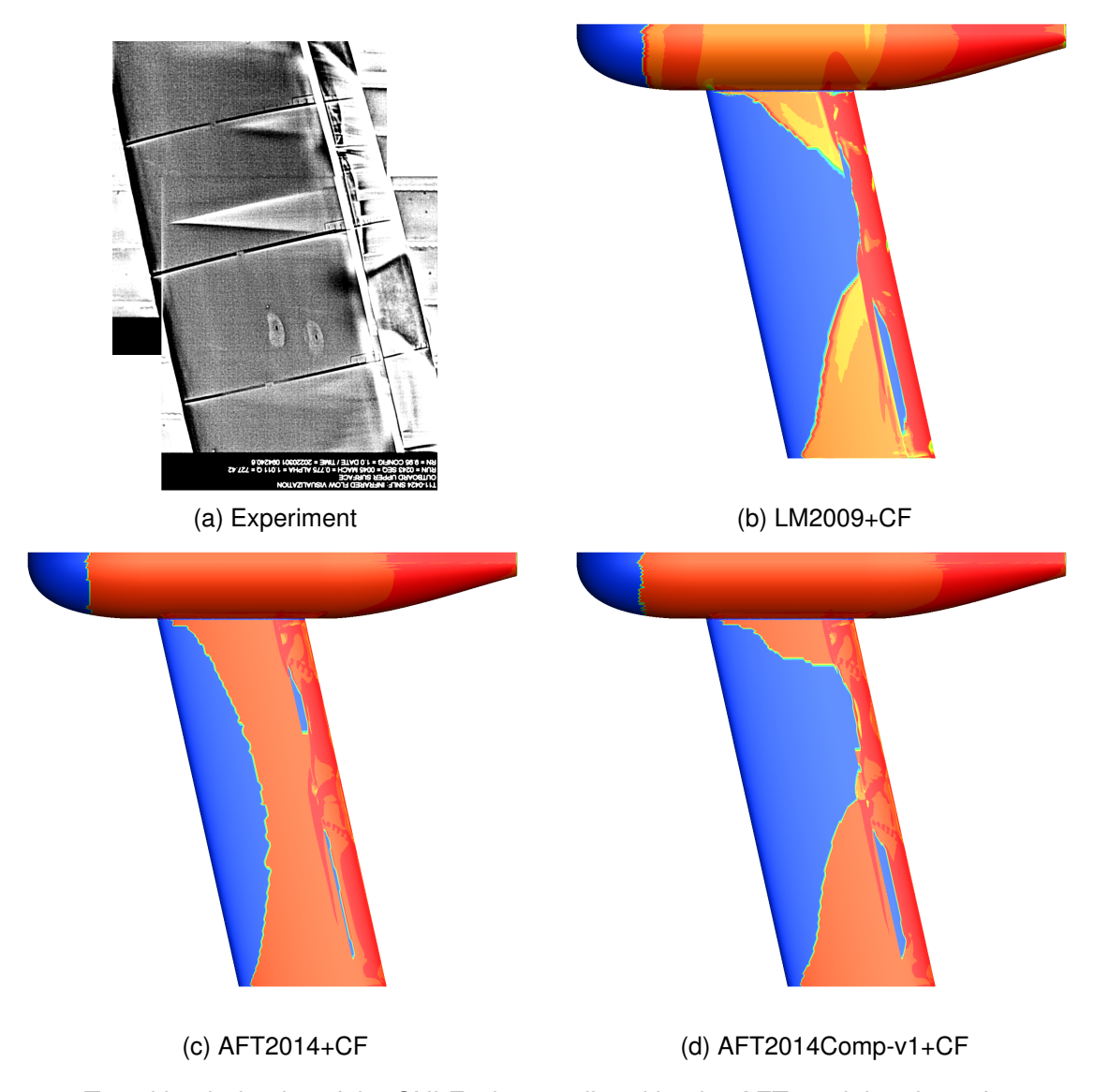


Figure 7 – Transition behavior of the SNLF wing predicted by the AFT model variants for M=0.775,  $Re=10\times10^6$ , and  $\alpha=1^\circ$ .

to one another. For  $\eta=0.6$  and inboard, the early transition is captured by all three models, and outboard of this, transition is caused by a shockwave. Nevertheless, there are key differences in the predictions. First, the AFT2019b model predicts transition furthest upstream, while Langtry-Menter predicts it furthers downstream. On the outboard section, the AFT2019b model captures an unexpected upstream transition due to the streamwise instability mechanism in a manner that is noticeably different than the AFT2014comp and Langtry-Menter models. Interestingly, the AFT2014comp model captures a slight delay in transition near the wing root downstream of the de-swept region. Neither the AFT2019b nor the Langtry-Menter models capture this behavior; however, it is present in the transition fronts reported by Lynde et al. [35].

A further comparison in the respective AFT-based results are included as Fig. 11, which depicts surface contours of the transported  $\tilde{n}$  variable as a "footprint" of the behavior higher in the boundary layer. There is a significant difference in the levels of the amplification factor between the AFT2019b and AFT2014Comp models, with the AFT2019b model being higher, which is consistent with the premature transition behavior observed for the S207, SNLF test case.

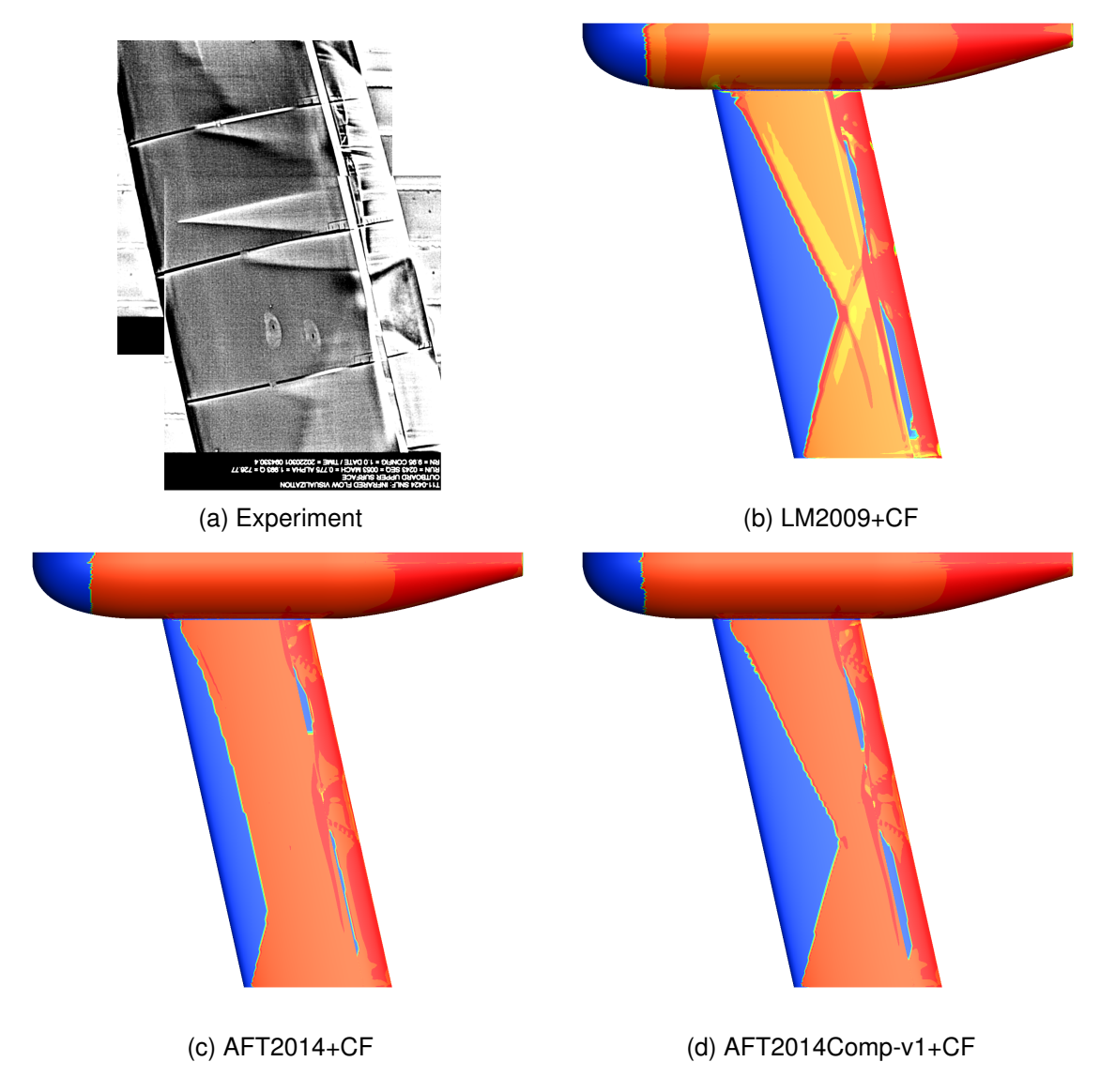


Figure 8 – Transition behavior of the SNLF wing predicted by the AFT model variants for M=0.775,  $Re=10\times10^6$ , and  $\alpha=2^\circ$ .

#### 5. Conclusion

Several prominent, PDE-based laminar-turbulent transition models implemented in the OVERFLOW solver have been evaluated in the context of natural-laminar-flow design at transonic flight conditions. As these common models are based primarily on incompressible arguments, their applicability for transonic NLF, where transition is expected to occur at or above sonic conditions, is not guaranteed. Recognizing this, two compressibility corrections were proposed and applied to the AFT2014 transition model. Through analysis of several test cases, some key trends emerged in the model behaviors.

For an NLF airfoil at low-speed conditions, the AFT2014 model was found to be most accurate, whereas the Langtry-Menter model was found to be least accurate. Most significantly, the free-stream turbulence decay effect of the SST turbulence model underlying the Langtry-Menter model contributes to an overprediction of laminar flow at off-nominal conditions. While it may be acceptable accuracy for analysis, such behavior can provide misleading guidance for new designs that lack experimental reference data. The AFT2019b model, on the other hand, underpredicted the laminar flow at off-nominal conditions and therefore underpredicted the maximum attainable lift-to-drag ratio.

When the models were applied to a transonic body of revolution, the baseline versions showed a pronounced lack of sensitivity to varying free-stream Mach numbers. The AFT2019b and Langtry-

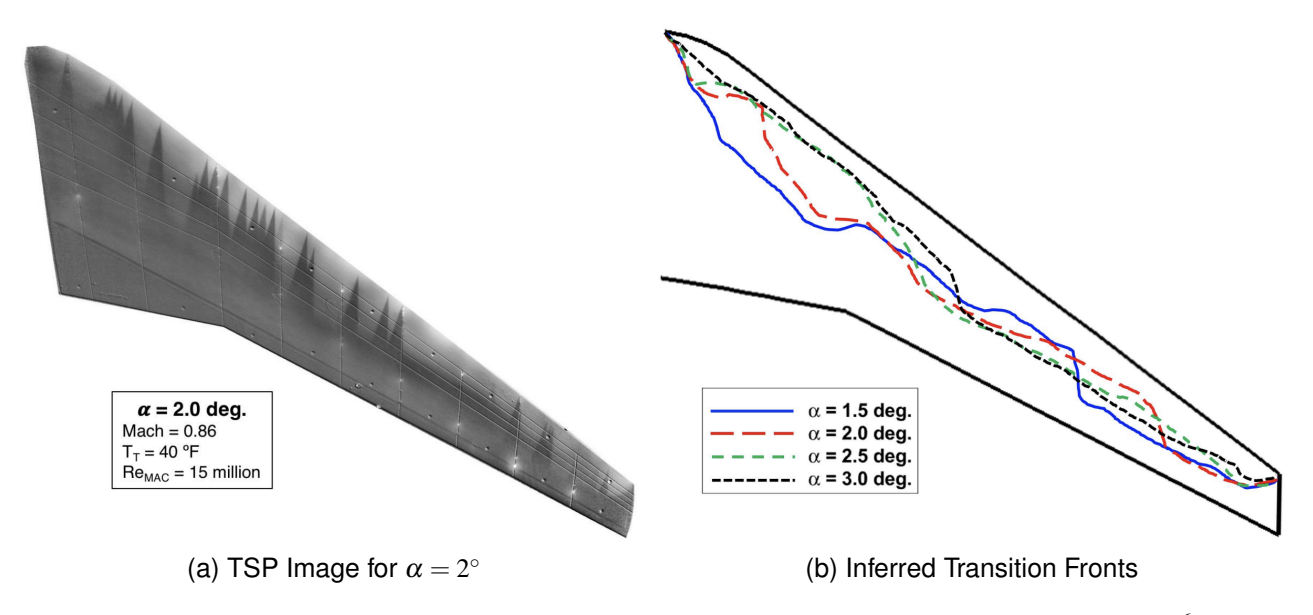


Figure 9 – Measured transition characteristics of the CRM-NLF at M=0.86,  $Re=15\times10^6$ , and  $\alpha=2^\circ$  (from Ref. [35]).

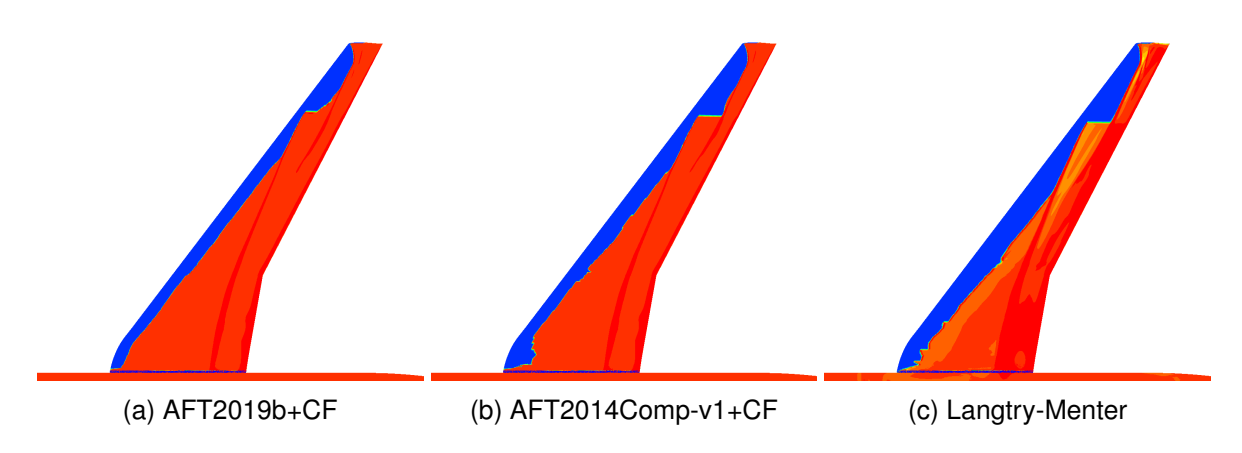


Figure 10 – Predicted transition characteristics of the CRM-NLF at M=0.86,  $Re=15\times10^6$ , and  $\alpha=2^\circ$ .

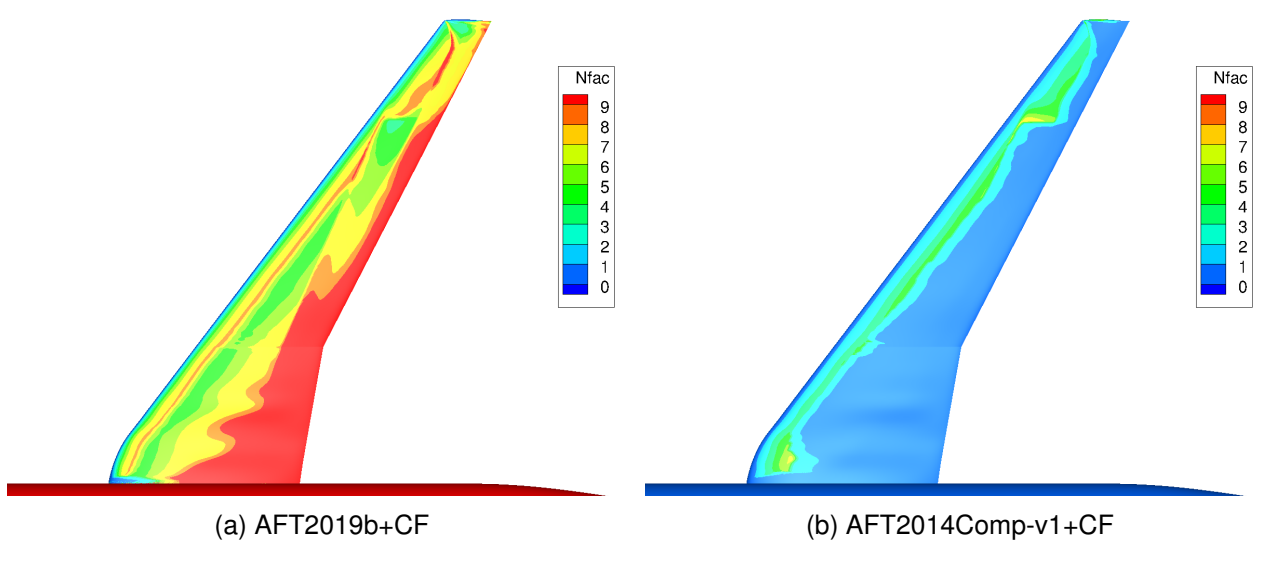


Figure 11 – Surface distribution of transported  $\tilde{n}$  variable for the CRM-NLF at M=0.86,  $Re=15\times10^6$ , and  $\alpha=2^\circ$ .

Menter models predicted nearly constant transition locations, with the Langtry-Menter transition being excessively far downstream. The baseline AFT2014 model showed some response to the changing Mach number, but transition was predicted too far upstream due to its lack of ability to damp instability growth in the presence of compressibility. Including compressibility corrections significantly improved the prediction accuracy, with the 'v1' correction performing best, and thus being the focus of subsequent analyses. The 'v2' correction showed the correct trends, and warrants further investigation in future work.

Application of the models to two separate transonic, NLF wing cases showed more-or-less consistent trends as the simpler cases. The AFT2014 model (without any compressibility correction) shows mild sensitivity to increasing Mach number, but transition remains premature. AFT2019b also showed premature transition. While this may seem counter to the results for the body of revolution for similar free-stream Mach numbers, one must keep in mind that the local Mach number on the wings is much higher and thus premature transition should be expected. The Langtry-Menter model predicted extensive laminar flow at the higher-Mach numbers, but sometimes erroneously so. As with the simpler cases, this is attributed to the free-stream turbulence decay. The AFT2014Comp-v1 model provided the most consistent results in terms of the absolute location of the transition front as well as the movement of transition with changing angle of attack and changing Mach number.

For the objective of transonic NLF design, the AFT2014Comp-v1+CF provided the best overall performance. It captures the sensitivity of transition to changing angle of attack (or lift coefficient) and changing Mach number better than the other models considered. Therefore, AFT2014Comp-v1+CF appears to be the model least likely to mislead a designer, but it is a model nevertheless.

## 6. Contact Author Email Address

mailto: jcoder@psu.edu

# 7. Copyright Statement

The author confirms that they, and/or their company or organization, hold copyright on all of the original material included in this paper. The author also confirms that they have obtained permission, from the copyright holder of any third party material included in this paper, to publish it as part of their paper. The author confirms that they give permission, or have obtained permission from the copyright holder of this paper, for the publication and distribution of this paper as part of the ICAS proceedings or as individual off-prints from the proceedings.

#### References

- [1] Michimasa Fujino, Yuichi Yoshizaki, and Yuichi Kawamura. "Natural-Laminar-Flow Airfoil Development for a Lightweight Business Jet". In: *Journal of Aircraft* 40.4 (2003), pp. 609–615.
- [2] Marty K. Bradley and Chris K. Droney. "Subsonic Ultra Green Aircraft Research: Phase I Final Report". In: *NASA/CR-2011-216847* (2011).
- [3] Marty K. Bradley and Chris K. Droney. "Subsonic Ultra Green Aircraft Research Phase II: N+4 Advanced Concept Development". In: NASA/CR-2012-217556 (2012).
- [4] Martin Kruse, Tobias Wunderlich, and Lars Heinrich. "A Conceptual Study of a Transonic NLF Transport Aircraft with Forward Swept Wings". In: *30th AIAA Applied Aerodynamics Conference*. New Orleans, LA: AIAA Paper 2012-3208, June 2012.
- [5] A. Seitz, A. Hübner, and K. Risse. "The DLR TuLam project: design of a short and medium range transport aircraft with forward swept NLF wing". In: *CEAS Aeronautical Journal* 11 (2020), pp. 449–459. DOI: 10.1007/s13272-019-00421-1.
- [6] Edward M. Greitzer et al. "N+3 Aircraft Concept Designs and Trade Studies, Final Report: Volume 1". In: NASA/CR-2010-216794/VOL1 (2010).

- [7] Michelle N. Lynde and Richard L. Campbell. "Computational Design and Analysis of a Transonic Natural Laminar Flow Wing for a Wind Tunnel Model". In: *35th AlAA Applied Aerodynamics Conference*. Denver, CO: AlAA Paper 2017-3058, June 2017. DOI: 10.2514/6.2017-3058.
- [8] Melissa B. Rivers et al. "Experimental Investigation of the NASA Common Research Model with a Natural Laminar Flow Wing in the NASA Langley National Transonic Facility". In: AIAA SciTech 2019 Forum. San Diego, CA: AIAA Paper 2019-2189, January 2019. DOI: 10.2514/ 6.2019-2189.
- [9] Richard L. Campbell and Michelle N. Lynde. "Natural Laminar Flow Design for Wings with Moderate Sweep". In: *34th AIAA Applied Aerodynamics Conference*. Washington, DC: AIAA Paper 2016-4326, June 2016. DOI: 10.2514/6.2016-4326.
- [10] Kristof Risse et al. "An Integrated Environment for Preliminary Aircraft Design and Optimization". In: 53rd AIAA/ASME/ASCE/AHS/ASC Structures, Structural Dynamics and Materials Conference. Honolulu, HI: AIAA Paper 2012-1675, April 2022.
- [11] J. G. Coder and M. D. Maughmer. "Computational Fluid Dynamics Compatible Transition Modeling Using an Amplification Factor Transport Equation". In: *AIAA Journal* (Vol. 52, No. 11, 2014, pp. 2506-2512). DOI: 10.2514/1.J052905.
- [12] J. G. Coder. "Further Development of the Amplification Factor Transport Transition Model for Aerodynamic Flows". In: *AIAA SciTech 2019 Forum* (AIAA Paper 2019-0039, San Diego, CA, January 2019). DOI: 10.2514/6.2019-0039.
- [13] Jared A. Carnes and James G. Coder. "Effect of Crossflow Transition on the Pressure-Sensitive-Paint Rotor in Hover". In: *Journal of Aircraft* 59.1 (2022), pp. 29–46. DOI: 10.2514/1. C036121.
- [14] R. B. Langtry and F. R. Menter. "Correlation-Based Transition Modeling for Unstructured Parallelized Computational Fluid Dynamics Codes". In: *AIAA Journal* (Vol. 47, No. 12, 2009, pp. 2894-2906.). DOI: 10.2514/1.42362.
- [15] R. B. Langtry et al. "Extending the  $\gamma$ -Re $_{\theta t}$  Local Correlation based Transition Model for Crossflow Effects". In: 45th AIAA Fluid Dynamics Conference (AIAA Paper 2015-2474, Dallas, TX, June 2015). DOI: 10.2514/6.2015-2474.
- [16] Balaji S. Venkatachari et al. "Transition Analysis for the CRM-NLF Wind Tunnel Configuration using Transport Equation Models and Linear Stability Correlations". In: *2022 AIAA SciTech Forum*. San Diego, CA: AIAA Paper 2022-1542, January 2022.
- [17] F. R. Menter et al. "A One-Equation Local Correlation-Based Transition Model". In: *Flow, Turbulence and Combustion* (Vol. 95, No. 4, 2015, pp. 583-619). DOI: 10.1007/s10494-015-9622-4.
- [18] J. G. Coder. "Enhancement of the Amplification Factor Transport Transition Modeling Framework". In: *55th AlAA Aerospace Sciences Meeting* (AlAA Paper 2017-1709, Grapevine, TX, January 2017). DOI: 10.2514/6.2017-1709.
- [19] P. R. Spalart and S. R. Allmaras. "A One-Equation Turbulence Model for Aerodynamic Flows". In: *Recherche Aerospatiale* (No. 1, 1994, pp. 5-21).
- [20] F. R. Menter. "Two-Equation Eddy-Viscosity Turbulence Models for Engineering Applications". In: *AIAA Journal* (Vol. 32, No. 8, 1994, pp. 1598-1605). DOI: 10.2514/3.12149.
- [21] Mark Drela. "A User's Guide to MSES 3.05". In: *MIT Department of Aeronautics and Astronautics* (July 2007).
- [22] Peter Sturdza. "An aerodynamic design method for supersonic natural laminar flow aircraft". PhD thesis. Stanford University, 2004.
- [23] Jared A. Carnes and James G. Coder. "Analyzing the Near-Wall Behavior of the Langtry–Menter Transition Model". In: *Flow, Turbulence and Combustion* 108.3 (Mar. 2022), pp. 683–715. DOI: 10.1007/s10494-021-00288-5.

- [24] R. H. Nichols and P. G. Buning. "User's Manual for OVERFLOW 2.4". In: (NASA Langley Research Center, Hampton, VA, July 2022). URL: https://overflow.larc.nasa.gov/.
- [25] P. L. Roe. "Approximate Riemann solvers, parameter, vectors and difference schemes". In: *Journal of Computational Physics* (Vol. 43, No. 2, 1981, pp. 357-372). DOI: 10.1016/0021-9991(81)90128-5.
- [26] Seokkwan Yoon and Antony Jameson. "Lower-upper Symmetric-Gauss-Seidel method for the Euler and Navier-Stokes equations". In: *AIAA Journal* 26.9 (1988), pp. 1025–1026. DOI: 10. 2514/3.10007.
- [27] Dan M. Somers. "Design and Experimental Results for a Natural-Laminar-Flow Airfoil for General Aviation Applications". In: *NASA TP-1861* (1981).
- [28] James G. Coder. "Standard Test Cases for CFD-Based Laminar-Transition Model Verification and Validation". In: 2018 AIAA Aerospace Sciences Meeting. Kissimmee, FL: AIAA Paper 2018-0029, January 2018. DOI: 10.2514/6.2018-0029.
- [29] Philippe R. Spalart and Christopher L. Rumsey. "Effective Inflow Conditions for Turbulence Models in Aerodynamic Calculations". In: *AIAA Journal* 45.10 (2007), pp. 2544–2553. DOI: 10.2514/1.29373.
- [30] Christopher L. Rumsey and Philippe R. Spalart. "Turbulence Model Behavior in Low Reynolds Number Regions of Aerodynamic Flowfields". In: *38th AIAA Fluid Dynamics Conference and Exhibit*. Seattle, WA: AIAA Paper 2008-4403, June 2008.
- [31] Boltz Frederick W, George C. Kenyon, and Clyde Q. Allen. "The boundary-layer transition characteristics of two bodies of revolution, a flat plate, and an unswept wing in a low-turbulence wind tunnel". In: NASA TN D-309 (1960).
- [32] Dan M. Somers. "Design of a Slotted, Natural-Laminar-Flow Airfoil for a Transport Aircraft". In: NASA/CR-2019-220403 (2019).
- [33] James G. Coder and Dan M. Somers. "Design of a slotted, natural-laminar-flow airfoil for commercial transport applications". In: *Aerospace Science and Technology* 106 (2020), p. 106217. DOI: 10.1016/j.ast.2020.106217.
- [34] J. G. Coder. "Transonic Wind-Tunnel Testing of a Slotted, Natural-Laminar-Flow Wing at Full-Scale Conditions". In: *AIAA SciTech 2023 Forum*. National Harbor, MD: AIAA Paper 2023-2452, January 2023.
- [35] Michelle N. Lynde, Richard L. Campbell, and Sally A. Viken. "Additional Findings from the Common Research Model Natural Laminar Flow Wind Tunnel Test". In: *2019 AIAA Aviation Forum.* Dallas, TX: AIAA Paper 2019-3292, June 2019. DOI: 10.2514/6.2019-3292.